

Anomalous valley Hall effect in electric-potential-difference antiferromagnetic Cr₂CHCl monolayer

Dun-Cheng Liang and San-Dong Guo*

School of Electronic Engineering, Xi'an University of Posts and Telecommunications, Xi'an 710121, China

Shaobo Chen

College of Electronic and Information Engineering,
Anshun University, Anshun 561000, Peoples Republic of China

The antiferromagnetic (AFM) valleytronics can be intrinsically more energy-saving and fast-operating in device applications. In general, the lacking spontaneous spin-splitting hinders the implementation and detection of anomalous valley Hall effect (AVHE). Here, we propose to implement AVHE in electric-potential-difference antiferromagnetic Cr₂CHCl monolayer with excellent stability, where the spontaneous spin-splitting can be induced due to layer-dependent electrostatic potential caused by out-of-plane built-in electric field. From a symmetry perspective, the introduction of Janus structure breaks the combined symmetry (PT symmetry) of spatial inversion (P) and time reversal (T), which gives rise to spin-splitting. Both unstrained and strained monolayer Cr₂CHCl possess valley splitting of larger than 51 meV, which is higher than the thermal energy of room temperature (25 meV). The layer-locked Berry curvature gives rise to layer-locked AVHE. Our work reveals a route to achieve AVHE in AFM monolayer with spontaneous spin-splitting.

I. INTRODUCTION

The discovery and successful preparation of rich two-dimensional (2D) materials lays the foundation for valleytronics, which can process information and perform logic operations with low power consumption and high speed[1–8]. Recently, the ferrovalley semiconductor (FVS) has been proposed to realize intrinsic valley polarization[9], which appears in out-of-plane hexagonal ferromagnetic (FM) materials with broken spatial inversion symmetry[9–18]. These offer interesting platforms to study valley-contrasting transport and Berry physics. In the FVS, valley-dependent Berry curvature can produce anomalous valley Hall effect (AVHE), where the charge Hall current originates from the spontaneous valley polarization. The antiferromagnetic (AFM) materials possess the high storage density, robustness against external magnetic field, as well as the ultrafast writing speed[19], so realizing valley polarization and AVHE in AFM materials is more meaningful for valleytronic application.

For 2D AFM materials with PT symmetry (a combined symmetry of spatial inversion (P) and time reversal (T)), there is zero berry curvature ($\Omega(k)$) and no spin-splitting everywhere in the momentum space, which hinders the realization of AVHE. Recently, an intuitive way is proposed to produce spin-splitting in AFM materials by making the magnetic atoms with opposite spin polarization locating in the different environment (surrounding atomic arrangement)[20]. The altermagnetism[21] and electric-potential-difference antiferromagnetism (EPD-AFM)[22] are the representative examples, and they possess intrinsic spin-splitting. For altermagnetism, the two different environments (The sur-

rounding atoms are in the same arrangement, yet not in the same orientation.) can be connected by special symmetry operation[21]. For EPD-AFM, the different environments occupied by two (spin-up and spin-down) magnetic atoms are due to an electric-potential-difference caused by an out-of-plane built-in electric field, and the magnetic atoms have opposite layer spin polarization (A-type AFM ordering). If EPD-AFM has hexagonal symmetry, the layer-locked Berry curvature can appear[23]. If hexagonal symmetry couples with the out-of-plane magnetization for EPD-AFM, spontaneous valley polarization will exist[23]. Therefore, an out-of-plane hexagonal EPD-AFM with energy extrema of conduction or valance bands located at high symmetry -K and K points can achieve AVHE.

The experimentally synthesized Cr₂C is a half-metallic ferromagnet[24]. By surface functionalization with H or Cl in Cr₂C, both ferromagnetic-antiferromagnetic transition and metal-insulator transition can be induced simultaneously[25]. The functionalized Cr₂CH₂ and Cr₂CCl₂ possess A-type AFM ordering and energy extrema at -K and K high symmetry points. However, for Cr₂CH₂ and Cr₂CCl₂, the spin degeneracy of -K and K valleys is maintained due to PT symmetry, which prohibits the AVHE. Based on Cr₂CH₂ and Cr₂CCl₂, a Janus Cr₂CHCl can be constructed to achieve hexagonal EPD-AFM, which is a possible candidate material to achieve AVHE.

II. COMPUTATIONAL DETAIL

Within density functional theory (DFT)[26], we perform the spin-polarized first-principles calculations within the projector augmented-wave (PAW) method, as implemented in Vienna ab initio Simulation Package

* sandongyuwang@163.com

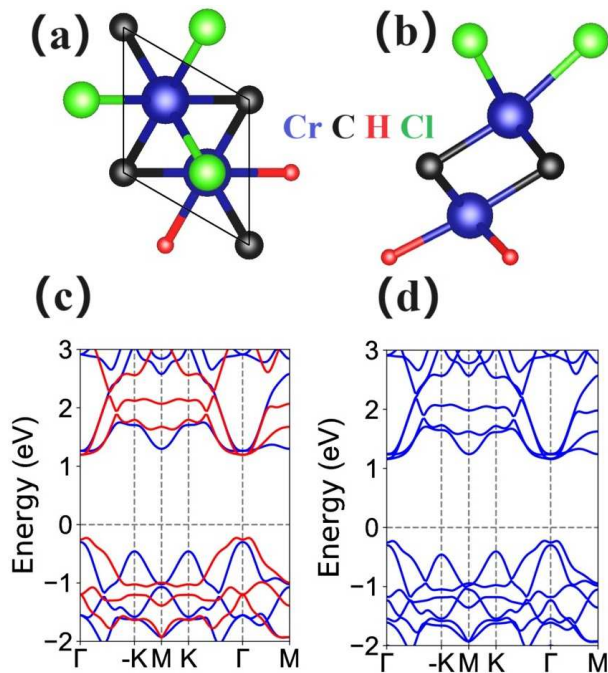


FIG. 1. (Color online) For monolayer Cr_2CHCl , the top (a) and side (b) views of crystal structures; the energy band structures without (c) and with (d) SOC. In (c), the spin-up and spin-down channels are depicted in blue and red.

(VASP)[27–29]. We use the generalized gradient approximation of Perdew-Burke-Ernzerhof (PBE-GGA)[30] as the exchange-correlation functional. The kinetic energy cutoff of 500 eV, total energy convergence criterion of 10^{-8} eV, and force convergence criterion of $0.0001 \text{ eV}\cdot\text{\AA}^{-1}$ are adopted. To account for the localized nature of Cr-3d orbitals, a Hubbard correction $U_{eff}=3.0 \text{ eV}$ [31, 32] is used by the rotationally invariant approach proposed by Dudarev et al[33]. The spin-orbital coupling (SOC) is included to investigate valley splitting and magnetic anisotropy energy (MAE). To avoid interactions between neighboring slabs, the vacuum space of more than 20 Å along z direction is added. We use a $21\times 21\times 1$ Monkhorst-Pack k-point meshes to sample the Brillouin zone (BZ) for calculating electronic structures. Based on finite displacement method with $5\times 5\times 1$ supercell, the interatomic force constants (IFCs) are calculated with AFM ordering, and the phonon dispersion is constructed by the Phonopy code[34]. The ab initio molecular dynamics (AIMD) simulations using NVT ensemble are performed with a $4\times 4\times 1$ supercell for more than 8000 fs with a time step of 1 fs. The Berry curvatures are calculated directly from the calculated wave functions based on Fukui’s method[35], as implemented in the VASPBERRY code[36–38].

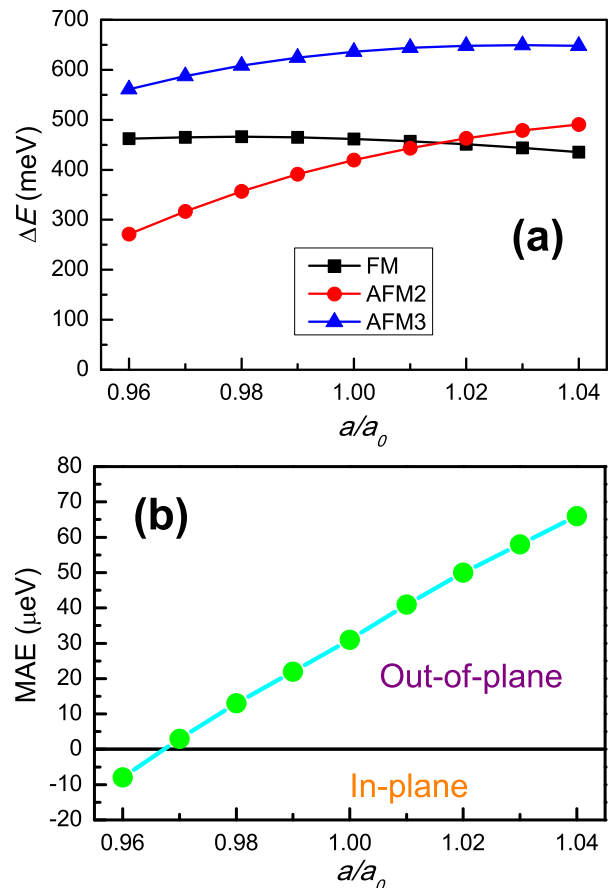


FIG. 2. (Color online) For Cr_2CHCl , the energy differences per unit cell between FM/AFM2/AFM3 and AFM1 (a) and MAE (b) as a function of a/a_0 .

III. CRYSTAL AND ELECTRONIC STRUCTURES

The Cr_2CH_2 and Cr_2CCl_2 monolayers have been proved to possess A-type AFM ordering with good stabilities[25]. Monolayer Cr_2CHCl can be constructed by replacing one of two H (Cl) layers with Cl (H) atoms in Cr_2CCH_2 (Cr_2CCl_2) monolayer. The crystal structures of Cr_2CHCl are shown in Figure 1 (a) and (b), which crystallizes in the $P3m1$ (No. 156), lacking spatial inversion symmetry. The Cr_2CHCl consists of five atomic layers in the sequence of H-Cr-C-Cr-Cl, which can produce built-in electric field due to special Janus structure. In addition, the magnetic Cr atoms of Cr_2CHCl distribute in two layers. These provide the basic conditions for EPD-AFM. The FM and three AFM configurations (AFM1, AFM2 and AFM3) are constructed, as shown in FIG.S1 of electronic supplementary information (ESI), to determine magnetic ground state of Cr_2CHCl . The AFM1 ordering is called A-type AFM state, which is necessary to form EPD-AFM. It is found that the energy of AFM1 per unit cell is 462 meV, 419 meV and 636 meV lower than those of FM, AFM2 and AFM3

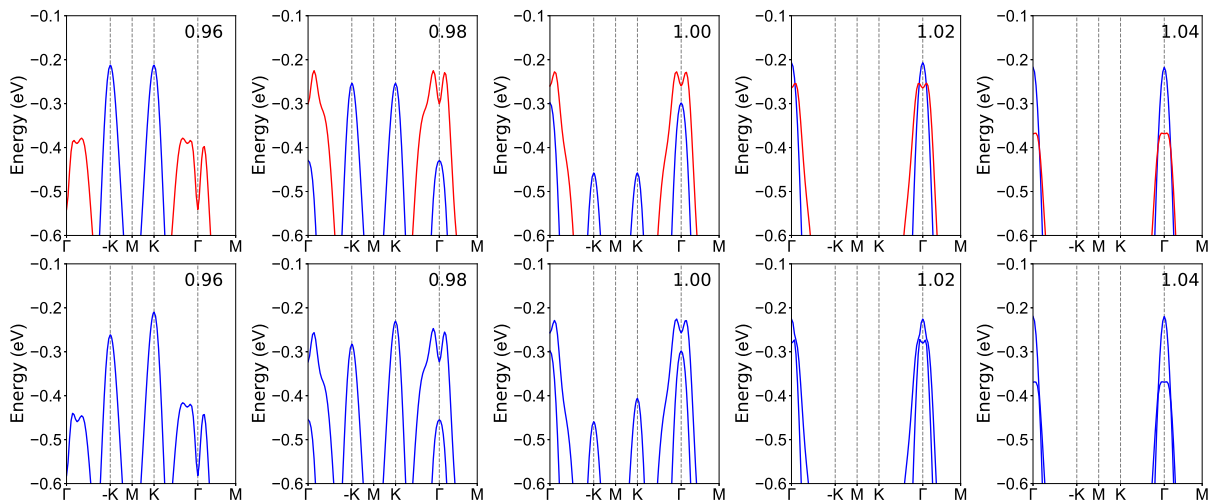


FIG. 3. (Color online) For Cr_2CHCl , the energy band structures of valence bands near the Fermi level without (top plane) and with (bottom plane) SOC at representative a/a_0 (0.96, 0.98, 1.00, 1.02 and 1.04). For top plane, the blue (red) lines represent the band structure in the spin-up (spin-down) direction.

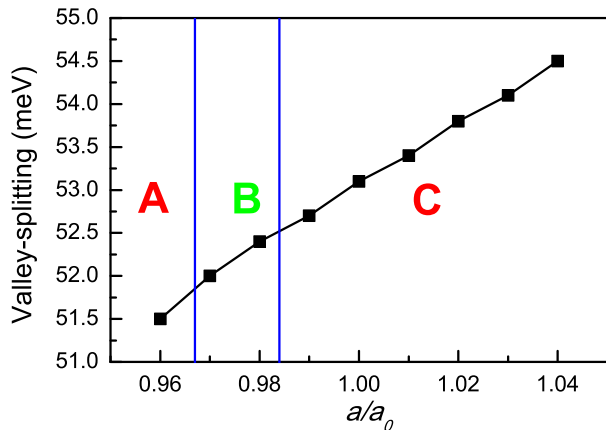


FIG. 4. (Color online) For Cr_2CHCl with assumed out-of-plane magnetization direction, the valley splitting as a function of a/a_0 . For region A, no spontaneous valley polarization appears due to the in-plane magnetization direction. For region C, the VBM is not at K/K point. For region B, it is suitable to produce AVHE.

cases within GGA+ U , confirming that the monolayer Cr_2CHCl possesses AFM1 ground state with the optimized equilibrium lattice constants $a=b=3.09$ Å. The calculated phonon spectrums of Cr_2CHCl show no obvious imaginary frequencies (see FIG.S2 of ESI), indicating its dynamic stability. Based on FIG.S3 of ESI, the AIMD simulation shows that the framework of Cr_2CHCl is well preserved with little fluctuations of total energy with increasing time during the simulation period, which confirms its thermal stability.

The magnetization direction is of great significance for generating spontaneous valley polarization, and only out-of-plane magnetization direction can produce spontaneous valley splitting[23]. The magnetic orientation

can be determined by calculating MAE, which can be calculated by $E_{MAE} = E_{SOC}^{\parallel} - E_{SOC}^{\perp}$. The E_{SOC}^{\parallel} and E_{SOC}^{\perp} are the energies that spins lie in-plane and out-of-plane, respectively. The calculated MAE is $31\mu\text{eV}/\text{unit cell}$, and the positive value indicates the out-of-plane easy magnetization axis of Cr_2CHCl , which means spontaneous valley polarization.

The energy band structures of Cr_2CHCl are plotted in Figure 1 (c) and (d) without SOC and with SOC for magnetization direction along the positive z direction. According to Figure 1 (c), the obvious spin-splitting can be observed due to the broken PT symmetry, and Cr_2CHCl is an indirect band gap semiconductor. For Cr_2CHCl , there are -K and K valleys with energy degeneracy in the valence band, but the valence band maximum (VBM) is not at the -K/K high symmetry point. The spin-splitting of Cr_2CHCl stems from a layer-dependent electrostatic potential, which occurs across the entire momentum space, producing the s -wave symmetry of spin-splitting[22]. This is different from altermagnetism (d , g , i -wave symmetry of spin-splitting) with momentum dependent spin-splitting[21]. When SOC is included, the spontaneous valley polarization with the valley splitting of 53 meV ($\Delta E_V = E_K^V - E_{-K}^V$) can be observed (Figure 1 (d)), and the energy of K valley is higher than one of -K valley. For Cr_2CHCl , the total magnetic moment per unit cell is strictly 0.00 μ_B , and the magnetic moment of bottom/top Cr atom is 3.13 μ_B /-3.06 μ_B . For EPD-AFM, the two types of magnetic (up and down) atoms cannot be connected by mirror or rotation symmetry, and the absolute values of their magnetic moments are not strictly equal, which is different from altermagnetism with strictly equal magnetic moments for up and down atoms[21].

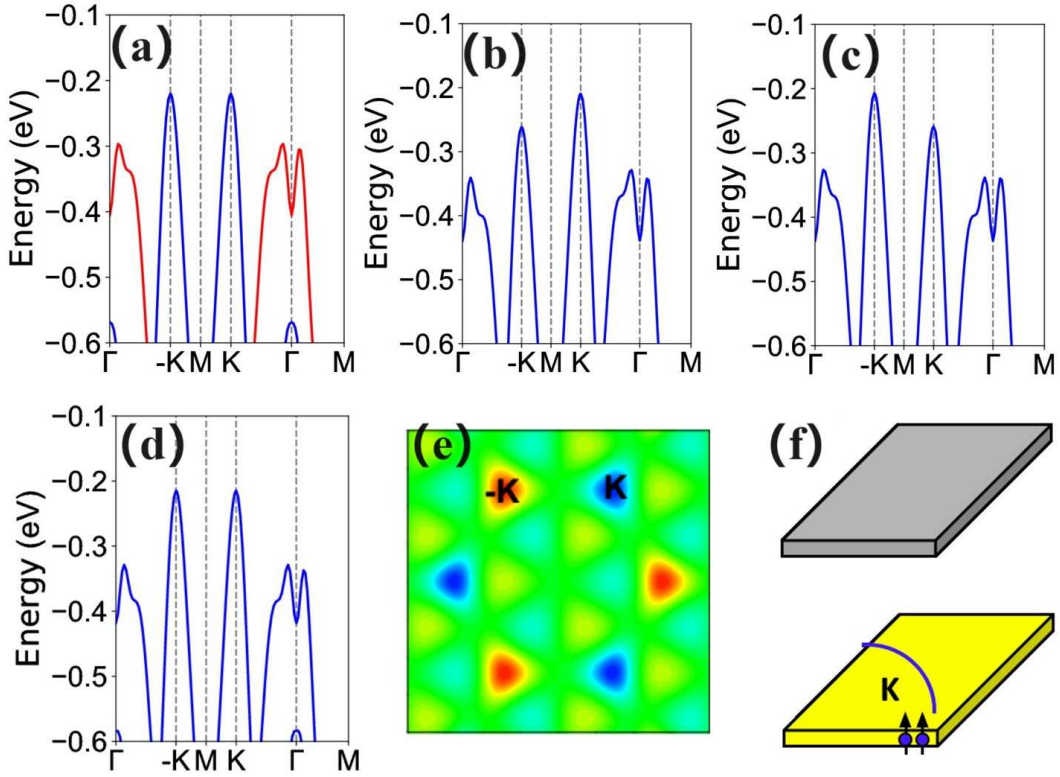


FIG. 5. (Color online) For Cr_2CHCl with $a/a_0=0.97$, the energy band structures without SOC (a), and with SOC (b, c, d) for magnetization direction along the positive z , negative z , and positive x direction, respectively; the distribution of Berry curvatures of spin-up (e); in the presence of a longitudinal in-plane electric field, an appropriate hole doping produces layer-locked AVHE (f), and the upper and lower planes represent the top and bottom Cr layers. In (a), the blue (red) lines represent the band structure in the spin-up (spin-down) direction.

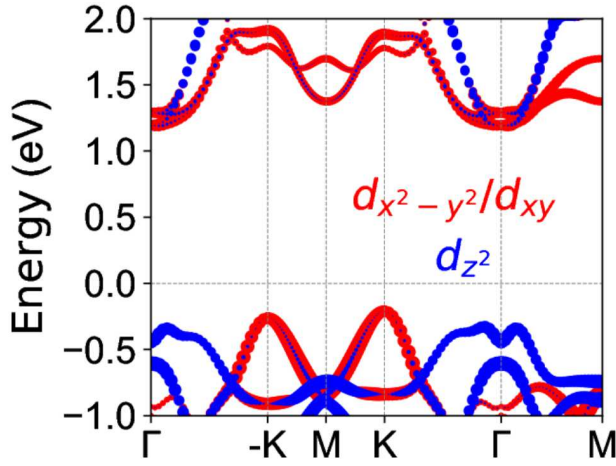


FIG. 6. (Color online) For Cr_2CHCl with $a/a_0=0.97$, Cr- d -orbital characters of energy bands within SOC.

IV. STRAIN EFFECTS

The VBM of Cr_2CHCl is not at the $-K/K$ high symmetry point, which is not conducive to implementation of AVHE. Strain is a very effective way to tune the po-

sition of energy extrema for 2D materials[39]. Here, the biaxial strain is applied to make VBM of Cr_2CHCl become $-K$ or K point. We use a/a_0 (0.96 to 1.04) to simulate the biaxial strain, and the $a/a_0 < 1$ ($a/a_0 > 1$) means the compressive (tensile) strain, where a and a_0 are the strained and unstrained lattice constants. Firstly, the magnetic ground state of strained Cr_2CHCl is determined by calculating energy differences (ΔE) between FM/AFM2/AFM3 and AFM1 states vs a/a_0 , as shown in Figure 2 (a). Within considered strain range, the positive ΔE confirm the AFM1 ground state of strained Cr_2CHCl .

The energy band structures of Cr_2CHCl at representative a/a_0 without SOC and with SOC (out-of-plane magnetization direction) are shown in FIG.S4 of ESI, and the enlarged figures of the valence band near the Fermi level are plotted in Figure 3. For valence band, the valley splitting as a function of a/a_0 are plotted in Figure 4. It is clearly seen that the $-K$ and K valleys always exist in the valence band, and they are from spin-up channel. It is found that the compressive strain can make $-K/K$ valley become VBM, and the critical point is approximately 0.984 for a/a_0 . The valley splitting of larger than 51 meV is maintained within considered a/a_0 range, and no valley polarization transition is produced. This is dif-

ferent from Janus GdClF monolayer[40], where the valley polarization transition can be driven by biaxial strain.

To achieve spontaneous valley splitting, another key factor is out-of-plane magnetization of strained Cr₂CHCl. The MAE as a function of a/a_0 is plotted in Figure 2 (b). It is found that compressive strain can induce the transition of magnetization direction, and the magnetization of Cr₂CHCl changes from out-of-plane case to in-plane case, when the a/a_0 is lower than 0.968. By considering the MAE and position of VBM together, Cr₂CHCl is suitable to produce AVHE, when the a/a_0 is between 0.968 and 0.984.

Taking $a/a_0=0.97$ as a example, the energy band structures of valence bands near the Fermi energy level without SOC and with SOC for magnetization direction along the positive z , negative z , and positive x directions are shown in Figure 5 (a), (b), (c) and (d). Figure 5 (a) shows obvious spin-splitting, and the VBM is at -K/K valley form the spin-up channel. However, no valley splitting can be observed. Figure 5 (b) shows the valley splitting of 52 meV, which is higher than the thermal energy of room temperature (25 meV). The energy of K valley is higher than one of -K valley. Figure 5 (c) indicates that the valley polarization transition can be achieved by reversing the magnetization direction. Figure 5 (d) shows that the in-plane magnetization direction produces no valley polarization.

The SOC-induced valley splitting is mainly from the intra-atomic interaction \hat{H}_{SOC}^0 (the interaction between the same spin states)[18]:

$$\hat{H}_{SOC}^0 = \lambda \hat{S}_z (\hat{L}_z \cos\theta + \frac{1}{2} \hat{L}_+ e^{-i\phi} \sin\theta + \frac{1}{2} \hat{L}_- e^{+i\phi} \sin\theta) \quad (1)$$

in which \hat{S} , \hat{L} and θ/ϕ mean the spin angular momentum, orbital angular momentum and the polar angles of spin orientation, respectively. For $d_{x^2-y^2}/d_{xy}$ -dominated -K/K valley with the group symmetry of C_{3h} , the valley splitting $\Delta E_V = 4\alpha \cos\theta$ [18], where the α is $\lambda|\hat{S}_z|$, and the $\theta=0/90^\circ$ means out-of-plane/in-plane direction. For Cr₂CHCl with $a/a_0=0.97$, the Cr- d -orbital characters of energy bands within SOC are plotted in Figure 6, which shows $d_{x^2-y^2}/d_{xy}$ -orbital-dominated -K and K val-

leys of valence bands. When the magnetization direction is along out-of-plane/in-plane case, the valley splitting of Cr₂CHCl will be $4\alpha/0$.

Due to A-type AFM ordering in Cr₂CHCl, the layer-locked Berry curvature can be observed[23]. Because -K and K valleys are from spin-up channel, the distribution of Berry curvatures of spin-up is shown in Figure 5 (e). It is clearly seen that the Berry curvatures are opposite for -K and K valleys. By applying a longitudinal in-plane electric field, the Bloch carriers will acquire an anomalous transverse velocity $v_\perp \sim E_\parallel \times \Omega(k)$ [41]. When the Fermi level is shifted between the -K and K valleys of the valence band, only the spin-up holes of K valley move to the bottom boundary of the sample under an in-plane electric field (Figure 5 (f)), producing layer-locked AVHE. This accumulation of spin-polarized holes produces a net charge/spin current, which will generate observable voltage.

V. CONCLUSION

In summary, we present a hexagonal AFM monolayer Cr₂CHCl with spontaneous spin-splitting to realize AVHE. The spontaneous valley polarization can occur in Cr₂CHCl with the valley splitting of larger than 51 meV due to intrinsic out-of-plane magnetization, when the a/a_0 is larger than 0.968. The introduction of a built-in electric field caused by Janus structure induces the spin-splitting in monolayer Cr₂CHCl due to layer-dependent electrostatic potential. By combining with layer-locked Berry curvature, the layer-locked AVHE can be achieved in monolayer Cr₂CHCl without applying out-of-plane external electric field. Our works enrich AFM valleytronic materials, and provide advantageous for the development of energy-efficient and ultrafast electronic devices.

ACKNOWLEDGMENTS

This work is supported by Natural Science Basis Research Plan in Shaanxi Province of China (2021JM-456). We are grateful to Shanxi Supercomputing Center of China, and the calculations were performed on TianHe-2.

-
- [1] J. R. Schaibley, H. Yu, G. Clark, P. Rivera, J. S. Ross, K. L. Seyler, W. Yao and X. Xu, Nat. Rev. Mater. **1**, 16055 (2016).
- [2] G. Pacchioni, Nat. Rev. Mater. **5**, 480 (2020).
- [3] S. A. Vitale, D. Nezhich, J. O. Varghese, P. Kim, N. Gedik, P. Jarillo-Herrero, D. Xiao and M. Rothschild, Small **14**, 1801483 (2018).
- [4] D. Xiao, M. C. Chang and Q. Niu, Rev. Mod. Phys. **82**, 1959 (2010).
- [5] T. Zhou, S. Cheng, M. Schleenvoigt, P. Schüffelgen, H. Jiang, Z. Yang and I. Žutić, Phys. Rev. Lett. **127**, 116402 (2021).
- [6] G. Xu, T. Zhou, B. Scharf and I. Žutić, Phys. Rev. Lett. **125**, 157402 (2020).
- [7] T. Zhou, J. Zhang, H. Jiang, I. Žutić and Z. Yang, npj Quant. Mater. **3**, 39 (2018).
- [8] T. Zhou, J. Zhang, B. Zhao, H. Zhang and Z. Yang, Nano Lett. **15**, 5149 (2015).
- [9] W. Y. Tong, S. J. Gong, X. Wan and C. G. Duan, Nat. Commun. **7**, 13612 (2016).
- [10] Y. B. Liu, T. Zhang, K. Y. Dou, W. H. Du, R. Peng, Y. Dai, B. B. Huang and Y. D. Ma, J. Phys. Chem. Lett. (2021).

- 12**, 8341 (2021).
- [11] Z. Song, X. Sun, J. Zheng, F. Pan, Y. Hou, M.-H. Yung, J. Yang and J. Lu, *Nanoscale* **10**, 13986 (2018).
- [12] J. Zhou, Y. P. Feng and L. Shen, *Phys. Rev. B* **102**, 180407(R) (2020).
- [13] P. Zhao, Y. Ma, C. Lei, H. Wang, B. Huang and Y. Dai, *Appl. Phys. Lett.* **115**, 261605 (2019).
- [14] X. Y. Feng, X. L. Xu, Z. L. He, R. Peng, Y. Dai, B. B. Huang and Y. D. Ma, *Phys. Rev. B* **104**, 075421 (2021).
- [15] Y. Zang, Y. Ma, R. Peng, H. Wang, B. Huang and Y. Dai, *Nano Res.* **14**, 834 (2021).
- [16] R. Peng, Y. Ma, X. Xu, Z. He, B. Huang and Y. Dai, *Phys. Rev. B* **102**, 035412 (2020).
- [17] W. Du, Y. Ma, R. Peng, H. Wang, B. Huang and Y. Dai, *J. Mater. Chem. C* **8**, 13220 (2020).
- [18] R. Li, J. W. Jiang, W. B. Mi and H. L. Bai, *Nanoscale* **13**, 14807 (2021).
- [19] T. Jungwirth, J. Sinova, A. Manchon, X. Marti, J. Wunderlich and C. Felser, *Nat. Phys.* **14**, 200 (2018).
- [20] S. D. Guo, Y. L. Tao, G. Z. Wang and Y. S. Ang, *J. Phys.: Condens. Matter* **36**, 215804 (2024).
- [21] L. Šmejkal, J. Sinova and T. Jungwirth, *Phys. Rev. X* **12**, 040501 (2022).
- [22] S. D. Guo and Y. S. Ang, *Phys. Rev. B* **108**, L180403 (2023).
- [23] S. D. Guo, L. Zhang, Y. Zhang, P. Li and G. Wang, *Phys. Rev. B* **110**, 024416 (2024).
- [24] B. Soundiraraju, R. Raghavan and B. K. George, *ACS Appl. Nano Mater.* **3**, 11007 (2020).
- [25] C. Si, J. Zhou and Z. Sun, *ACS Appl. Mater. Interfaces* **7**, 17510 (2015).
- [26] P. Hohenberg and W. Kohn, *Phys. Rev.* **136**, B864 (1964); W. Kohn and L. J. Sham, *Phys. Rev.* **140**, A1133 (1965).
- [27] G. Kresse, *J. Non-Cryst. Solids* **193**, 222 (1995).
- [28] G. Kresse and J. Furthmüller, *Comput. Mater. Sci.* **6**, **15** (1996).
- [29] G. Kresse and D. Joubert, *Phys. Rev. B* **59**, 1758 (1999).
- [30] J. P. Perdew, K. Burke and M. Ernzerhof, *Phys. Rev. Lett.* **77**, 3865 (1996).
- [31] T. Zhao, S. Xing, J. Zhou, N. Miao and Z. Sun, *Journal of Materiomics* **10**, 269 (2024).
- [32] J. He, G. Ding, C. Zhong, S. Li, D. Li and G. Zhang, *Nanoscale*, **11**, 356 (2018).
- [33] S. L. Dudarev, G. A. Botton, S. Y. Savrasov, C. J. Humphreys and A. P. Sutton, *Phys. Rev. B* **57**, 1505 (1998).
- [34] A. Togo, F. Oba and I. Tanaka, *Phys. Rev. B* **78**, 134106 (2008).
- [35] T. Fukui, Y. Hatsugai and H. Suzuki, *J. Phys. Soc. Japan.* **74**, 1674 (2005).
- [36] H. J. Kim, <https://github.com/Infant83/VASPBERRY>, (2018).
- [37] H. J. Kim, C. Li, J. Feng, J.-H. Cho and Z. Zhang, *Phys. Rev. B* **93**, 041404(R) (2016).
- [38] S. W. Kim, H. J. Kim, S. Cheon and T. H. Kim, *Phys. Rev. Lett.* **128**, 046401 (2022).
- [39] S. D. Guo, *J. Mater. Chem. C* **4**, 9366 (2016).
- [40] S. D. Guo, X. S. Guo, X. X. Cai and B. G. Liu, *Phys. Chem. Chem. Phys.* **24**, 715 (2022).
- [41] D. Xiao, M. C. Chang and Q. Niu, *Rev. Mod. Phys.* **82**, 1959 (2010).